



HAL
open science

Wavelength scaling of ultrafast demagnetization in Co/Pt multilayers

Vincent Cardin, Tadas Balciunas, Katherine Légaré, Andrius Baltuska, Heide Ibrahim, Emmanuelle Jal, Boris Vodungbo, Nicolas Jaouen, Charles Varin, Jan Lüning, et al.

► **To cite this version:**

Vincent Cardin, Tadas Balciunas, Katherine Légaré, Andrius Baltuska, Heide Ibrahim, et al.. Wavelength scaling of ultrafast demagnetization in Co/Pt multilayers. *Physical Review B*, 2020, 101 (5), pp.054430. 10.1103/PhysRevB.101.054430 . hal-03058588

HAL Id: hal-03058588




<https://hal.sorbonne-universite.fr/hal-03058588v1>

Submitted on 26 Feb 2021

HAL is a multi-disciplinary open access archive for the deposit and dissemination of scientific research documents, whether they are published or not. The documents may come from teaching and research institutions in France or abroad, or from public or private research centers.

L'archive ouverte pluridisciplinaire **HAL**, est destinée au dépôt et à la diffusion de documents scientifiques de niveau recherche, publiés ou non, émanant des établissements d'enseignement et de recherche français ou étrangers, des laboratoires publics ou privés.

Wavelength scaling of ultrafast demagnetization in Co/Pt multilayers

Vincent Cardin ¹, Tadas Balciunas,² Katherine Légaré,¹ Andrius Baltuska,² Heide Ibrahim ¹, Emmanuelle Jal ³,
Boris Vodungbo,³ Nicolas Jaouen,⁴ Charles Varin,⁵ Jan Lüning,³ and François Légaré¹

¹*INRS-EMT, 1650 boulevard Lionel-Boulet, Varennes, Québec, Canada J3X1S2*

²*TU WIEN, Faculty of Electrical Engineering, Gußhausstrasse 25–29, 1040 Wien, Austria*

³*Sorbonne Université, CNRS, Laboratoire de Chimie Physique–Matière et Rayonnement, LCPMR, 75005 Paris, France*

⁴*Synchrotron SOLEIL, L'Orme des Merisiers, 91190 Saint-Aubin, France*

⁵*Cégep de l'Outaouais, Gatineau, Québec, Canada J8Y 6M4*



(Received 19 August 2019; revised manuscript received 27 January 2020; accepted 28 January 2020; published 21 February 2020; corrected 28 February 2020)

Ultrafast demagnetization, a phenomenon of utmost interest in the context of optical control of magnetically recorded data, has been extensively studied in a variety of different materials. However, only a limited number of studies have investigated the impact of the pump laser wavelength on the process, and only within a narrow spectral range. Performing resonant scattering experiment at the cobalt $M_{2,3}$ edges, using extreme ultraviolet radiation photons from a high harmonic source, we studied the ultrafast demagnetization dynamics of Co/Pt multilayers by tuning the pump wavelength to 0.4, 0.8, and 1.8 μm . We show that the degree of demagnetization at short time scale (100s of fs) is stronger at longer wavelengths. This is explained by the wavelength dependence of both the laser induced heating of the electrons ($T_e \propto \lambda^2$) and the spatial distribution of the electromagnetic energy deposited into the multilayer sample.

DOI: [10.1103/PhysRevB.101.054430](https://doi.org/10.1103/PhysRevB.101.054430)

I. INTRODUCTION

In 1996, Beaurepaire *et al.* [1] discovered ultrafast demagnetization as a femtosecond laser driven process. More recently, coherent control of magnetization has been demonstrated using THz pulses [2,3], where the magnetic moment of the material follows the magnetic field of the optical excitation. However, for the vast majority of reported cases, the exact nature of the electromagnetic field driving the process (the pump pulse) has not been considered. Previous work considered the energy dependence of the ultrafast magnetization probe, e.g., to study the spin-polarized electrons energy compared to the Fermi level [4], or to separate the optical coherent effects from the true magnetization response of a material when the magneto-optic Kerr effect (MOKE) is used for probing [5]. In comparison, most studies gave no consideration to the effect of the pump wavelength, with a few exceptions [6–8], and simply used the most available femtosecond technology, the titanium-sapphire laser ($\lambda \sim 0.8 \mu\text{m}$).

The creation of hot, conducting electrons is recognized as the first step of the demagnetization sequence [4,9–13]. It has been recently shown using *ab initio* calculations [14] that the early onset of demagnetization is dominated by electronic processes. Tengdin *et al.* [15] provide evidence that the demagnetization is driven by an optically excited transient increase of the electronic temperature. Furthermore, the importance of the temperature distribution of these hot electrons has recently been shown to play a major role in demagnetization [15–17]. It has been demonstrated that magnetization can be quenched via an indirect excitation by hot electrons optically created in an infrared (IR)-opaque capping layer [16,18–20]. In the case of such indirect excitation, super-diffusion of nonthermal

[16,19] or diffusion of thermal [18,20] hot electrons from this capping layer into the magnetic structure initiate the ultrafast demagnetization. In the case of direct excitation, we expect the wavelength of the pump pulse to have an effect on the energy transfer to the hot electrons responsible for the process.

II. EXPERIMENT & RESULTS

We investigate the pump-wavelength dependence of the ultrafast demagnetization of a Co/Pt multilayer sample ($\text{SiN}_{30}/\text{Pt}_2/[\text{Co}_{0.6}\text{Pt}_{0.8}]_{30}/\text{Al}_3$) using pump with wavelengths of 0.4, 0.8, and 1.8 μm . HHG-based x-ray resonant magnetic scattering (XRMS) at the cobalt M edge (60 eV) was used to probe the magnetization dynamics. The pump-probe experiment is schematized in Fig. 1 and more details are provided in the Supplemental Material. We observe a significant wavelength dependence of the maximum degree of magnetization quenching at constant absorbed energy, with a stronger quenching for longer pump wavelength.

Results for the initial 2.5 ps delays at a variety of pump fluences for the three wavelengths are shown as symbols in Figs. 2(a), 2(b), and 2(c). In order to recover the wavelength scaling, the indicated fluences are corrected by the loss from sample reflections, and therefore correspond to the absorbed fluence. All the curves shown in Fig. 2 exhibit the characteristic behavior of a sharp decay within hundreds of fs, followed by a slower partial magnetization recovery. The time at which the maximum quenching of the magnetization occurs (minimum of the curve) appears to be wavelength and intensity independent at ~ 230 fs. While the curves for pump at 0.4 and 0.8 μm show an almost linear recovery (a) and (b), the curves for 1.8 μm (c) exhibit a more pronounced curvature and a faster recovery.

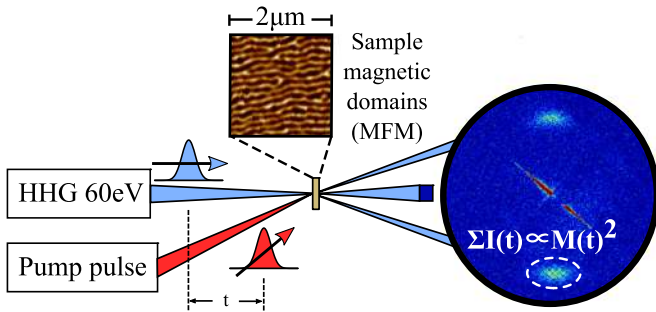


FIG. 1. Conceptualization of the pump-probe XRRMS technique. The pump (red) reach the sample at a time t before the 60-eV photons (blue). The pump affects the sample magnetization. The 60-eV photons are diffracted by the striped magnetic domain. The intensity of the diffracted peak is proportional to the transmission of the sample and the second power of its magnetization at time t [21].

We have fitted these results with an empirical model (dashed lines) based on convolution of a normalized Gaussian pulse with a bi-exponential decay [21–23]. The model describing the evolution of the normalized magnetization $M(t)/M_0$ yields the characteristic time scales of the magnetization quenching (demagnetization time, τ_1) and the slower partial recovery (recovery time, τ_2). The parameters τ_1 and τ_2 are illustrated in Fig. 2(e):

$$\frac{M(t)}{M_0} = G(t) \otimes \left[1 - H(t) \left[B \left(1 - \exp\left(\frac{-t}{\tau_1}\right) \right) \exp\left(\frac{-t}{\tau_2}\right) + C \left(1 - \exp\left(\frac{-t}{\tau_2}\right) \right) \right] \right], \quad (1)$$

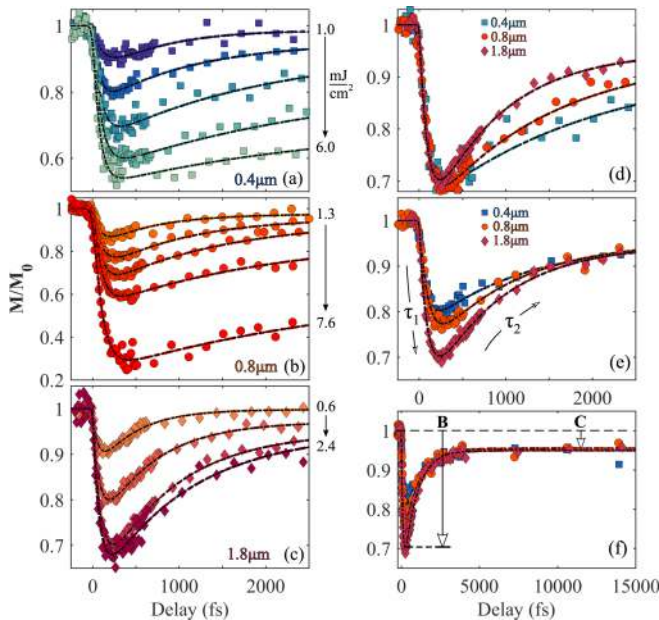


FIG. 2. Demagnetization curves for the three pump wavelengths (a) $0.4 \mu\text{m}$, (b) $0.8 \mu\text{m}$, (c) $1.8 \mu\text{m}$. (d) Comparison of dynamics at different wavelengths for the same maximum quenching, \mathbf{B} . (e) Comparison of curves showing the same long-term magnetization level \mathbf{C} . (f) Same curves as (e) for the complete measured pump-probe delay. The fitting parameters are illustrated in (e) and (f).

where $H(t)$ is the Heavyside function. The parameter \mathbf{B} primarily determines the maximum quenching of the magnetization, $1 - (M/M_0)_{\min}$. Parameter \mathbf{C} represents the asymptotic demagnetization at long delays, i.e., the higher \mathbf{C} , the lower the recovered magnetization [see Fig. 2(f) where \mathbf{B} and \mathbf{C} are represented].

For comparison reasons, we grouped the measurement data either by the maximum demagnetization (constant \mathbf{B}) or by the constant asymptotic magnetization level (constant \mathbf{C}). Demagnetization dynamics measurements in Fig. 2(d) show the curves for the three pump wavelengths of identical maximum quenching. It indicates a faster recovery for the longer wavelength for the same level of magnetization quenching. Conversely, Fig. 2(e) is grouped for comparison of curves that reach the same value of demagnetization at long delays (constant parameter \mathbf{C}). One notes that the $1.8\text{-}\mu\text{m}$ -pumped curve exhibits the highest level of magnetization quenching (parameter \mathbf{B}), followed by the $0.8 \mu\text{m}$ and then the $0.4 \mu\text{m}$. Figure 2(f) shows the same curves as Fig. 2(e), but over the full range of the measured pump-probe delays up to 13 ps.

III. DISCUSSION

A. Alternative energy gauges

Our results indicate that either the initial demagnetization, its recovery, or both are being influenced by the pump wavelength. In order to avoid inaccuracies from a separate measurement of the absolute pump fluences, we introduce two gauges for the energy absorbed by the system. These gauges are independent of experimental conditions and consist in (i) the recovery time, τ_2 , and (ii) the remaining demagnetization at long delays, \mathbf{C} . The maximum magnetization quenching, \mathbf{B} , is then evaluated as a function of these gauges in Fig. 3. In Fig. 3(a), the dependence of \mathbf{B} over the recovery time, τ_2 , is approximated with a linear function. In Fig. 3(b), the maximum demagnetization, \mathbf{B} , is depicted as a function of the remaining demagnetization at long delays, \mathbf{C} . It is empirically fitted by a square root function. The insets of both panels show the empirical fitting parameters as a function of wavelength. In both cases, the maximum quenching of magnetization at early time (\mathbf{B}) increases with increasing pump wavelength.

Such different scaling behavior of \mathbf{B} vs \mathbf{C} and \mathbf{B} vs τ_2 is expected. Although parameter \mathbf{C} is clearly linked to the absorbed energy, their relation at very low and very large pump fluence is uncertain. At very low pump fluence, the recovery is fast enough for the asymptotic-like value of the magnetization between ≈ 2.5 and 13 ps to be zero, while parameter \mathbf{B} is nonzero. Additionally, as the quenching of magnetization saturates for large pump fluences, the parameter \mathbf{B} levels off while parameter \mathbf{C} keeps increasing, leading to a radical-like function.

The recovery time, τ_2 , however, represents a physical quantity more directly related to the absorbed energy, as an excited system will unequivocally recover over a certain time. The linear dependence of τ_2 with the pump fluence has been extensively observed [15,21,24,25]. An explanation is that the specific heat of the electron bath increases with increasing temperature, reducing heat transfer rate to the phonons for high fluences [26,27]. In our study, τ_2 is also found to

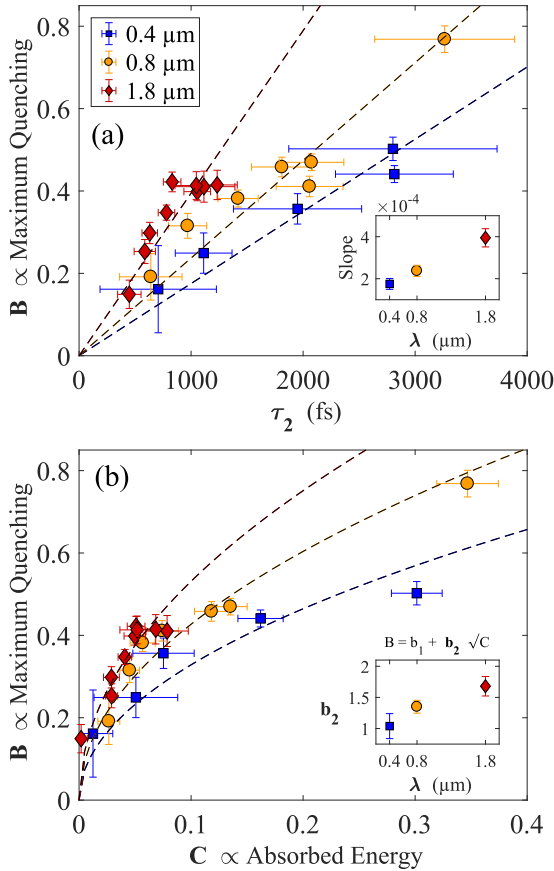


FIG. 3. Wavelength dependence ($0.4 \mu\text{m}$ in blue, $0.8 \mu\text{m}$ in orange, $1.8 \mu\text{m}$ in red) of the maximum magnetization quenching \mathbf{B} and the alternative energy gauges \mathbf{C} , and τ_2 [c.f. Eq. (1)]. The dashed lines represent an empirical extrapolation of the data points. Each data point represents a full demagnetization curve. Panel (a) shows the maximum quenching \mathbf{B} in relation to the relaxation time, τ_2 . Panel (b) depicts the maximum quenching of the magnetization \mathbf{B} in relation to the asymptotic demagnetization \mathbf{C} . The insets of panel (a) and (b) represent the fitting parameters for both empirical fitting equations.

increase linearly with the measured fluence for all wavelengths [28]. Additionally, since the recovery of the magnetization begins long after the pump, it should be unaffected by any wavelength-dependent material effect. Hence, in the context of investigating a wavelength scaling of the ultrafast demagnetization, we argue that τ_2 is a more intrinsic gauge of the effective fluence reaching the material.

For the reasons stated above, both gauges cannot have the same relationship to the absorbed energy in the system, although they undoubtedly share a dependence to it. Plotting \mathbf{C} against τ_2 for the three wavelengths [28] shows that both gauges are independent of the pump wavelength. This can be explained by the fact that, far from a phonon resonance, the rate of the energy dissipation is a property of the material that is expected to be completely independent of the photon wavelength. The time it takes for the energy to dissipate (τ_2), or equivalently, the asymptotic magnetization at long delays (parameter \mathbf{C}), should only depend on the energy absorbed by the system. These assumptions are consistent

with the demagnetization measurements of a directly and indirectly excited similar Co/Pt multilayer [20], where no discernable differences in the dynamics of magnetization recovery have been observed, despite the very different nature of the initial excitation.

B. Drude model with dispersion

Explaining these results with a complete model would be extremely challenging as it would require starting from first principles, i.e., dealing with the multibody electron, phonon, and spin wave function coupled with the laser pulse's electromagnetic wave propagation across multiple material interfaces and throughout the entire sample. So far, experiments were explained successfully with Beaurepaire's [1] phenomenological three-temperature model (3T) that tracks the evolution of the average energy of the electron, spin, and phonon (ESP) populations in terms of the ESP temperatures T_e , T_s , and T_p . Within the 3T perspective, the individual ESP populations are assumed to be in an internal thermal equilibrium at all times and the laser-induced demagnetization proceeds as follows. First, on the time scale of the pulse, electrons are heated by the laser with negligible energy exchange with the spin and phonon populations. In a second step, excess electronic energy is transferred to the spins, reaching a maximum of demagnetization on the subpicosecond time scale. Finally, as the three populations evolve toward a thermal equilibrium, magnetization is partially recovered. Demagnetization on the multipicosecond time scale [\mathbf{C} , see Fig. 2(f)] is proportional to the energy deposited into the sample. For moderate heating, it is possible to show that the maximum electron temperature reached after the pump pulse is proportional to the fluence F Ref. to SI ([28]):

$$\Delta T_{e,\text{max}} = \sqrt{T_{e,0}^2 + \frac{2}{\gamma}W} - T_{e,0} \cong \frac{W}{C_e(T_{e,0})}, \quad (2)$$

where $T_{e,0}$ is the initial electron temperature, and γ is the electronic specific heat constant such that $C_e(T_e) = \gamma T_e$, and $W = 2\pi\epsilon_2 F/\lambda$ is the energy density transferred to the medium with a relative permittivity $\epsilon_r = \epsilon_1 + i\epsilon_2$. We stress that with this definition of W , both F and λ are defined in vacuum. In most studies so far, the term $2\pi\epsilon_2/\lambda$ was assumed to be constant, leaving the long-term demagnetization to depend only upon the laser fluence F . However, it appears clearly here that the laser-induced demagnetization dynamics should also be influenced by the pump wavelength λ , for the simple reason that materials are optically dispersive, i.e., that the value of their relative permittivity changes with the wavelength.

We computed an effective sample permittivity sample by weighting the contribution from the individual materials with respect to their relative volume and observed that energy absorption globally scales with λ^2 Ref. to SI ([28]). We can link this trend to a more effective heating of the conduction electrons at longer wavelengths via intraband transitions. For instance, for the wavelength range considered in the experiments, the weighted, effective optical response is fairly represented by a Drude permittivity and it is possible to show that the cycle-averaged optical power absorbed by the conduction

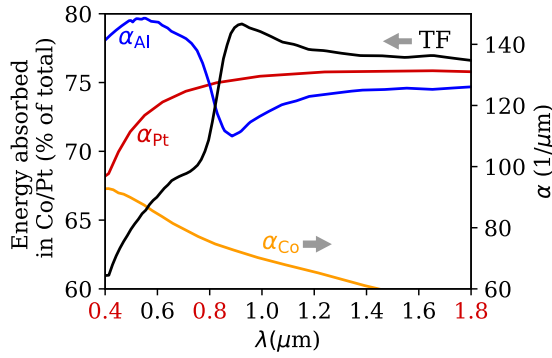


FIG. 4. Optical absorption data for Al [29], Pt [30], and Co [31] reveal a strong dependence with regards to the laser wavelength. Estimations based on the Beer-Lambert law (see text) and the thin-film electromagnetic theory (TF, black line) show that with increasing wavelength more energy gets deposited in the Co/Pt part of the sample.

electrons can be approximated by the following equation:

$$\left\langle \frac{dW}{dt} \right\rangle = \frac{1}{2} \left(\frac{\sigma}{1 + \omega^2 \tau^2} \right) E_0^2 \cong \frac{2N}{\tau} U_p \propto \lambda^2, \quad (3)$$

where σ is the static conductivity, $\omega = 2\pi c/\lambda$ is the angular frequency, τ is the electron collision mean free time, E_0 is the amplitude of the electric field, N is the density of conduction electrons, and $U_p = e^2 E_0^2 / 4m\omega^2$ is the ponderomotive energy of a free electron oscillating in the field, with e being the elementary electric charge and m the electron mass. The λ^2 -scaling trend indicates that, for a given pulse energy, electron heating and subsequent demagnetization should be more efficient using longer wavelengths. This is supported by our observations of a higher level of demagnetization at early times for 1.8 μm . Note that in the limit where $\omega = 0$, the equation above is equivalent to the static source term $P(t)$ of Beaupaire's [1].

C. Optical absorption in the multilayers

Further insight was gained by looking at optical data for Al [29], Pt [30], and Co [31], from which we computed the decay constant $\alpha = 2\pi\kappa/\lambda$ as a function of the wavelength λ (n and κ are the refractive index and extinction index, such that $\epsilon_r = (n + i\kappa)^2$). We consider an oxidation layer (Al_2O_3) of 1.5 nm [32–34], reducing the effective thickness of the aluminum capping layer to 1.5 nm.

It is noted that the optical data from the above references was obtained from films with different thickness compared to our sample. It is known that for nanoscale objects like thin films, optical properties are strongly influenced by the size of the object, e.g., by the thickness [35]. The current analysis provides an intuitive picture to explain our results, but should be interpreted with care. Nevertheless, from the results summarized in Fig. 4, it stands out that optical absorption in the three investigated conductive materials varies significantly over the 0.4–1.8 μm and favors direct energy deposition in Co/Pt when increasing the wavelength from 0.4 to 1.8 μm .

In order to get a qualitative insight, we first used the Beer-Lambert law. At first glance, it suggests that more than 80% of the pulse energy transmitted into the sample is effectively

deposited into the Co/Pt layers [28] and that the dependence of this transmitted energy with the wavelength is not strong (within 2%). However, including multiple optical reflections at the Al-Pt and Al-air interfaces reduces the fraction reaching the Co/Pt layers down to 70% while increasing the wavelength dependence to $\sim 7\%$. To fully assess optical reflections and multiple beam interference in the entire sample, we used the thin-film electromagnetic theory [36]. The complete theory clearly shows that out of a given pulse energy reaching the Co/Pt layer, about 15% more gets absorbed at 1.8 μm compared to 0.4 μm (thin-film results are labeled TF in Fig. 4).

From this analysis, it stands out that for a given pulse energy deposited into the sample, a higher fraction is effectively absorbed within the Co/Pt at 1.8 μm , followed by 0.8, and 0.4 μm . At short time scales, an increasing transient electron temperature is reached in the magnetic region of the sample for longer pump wavelength thus leading to a stronger quenching of the magnetization at short time scales [B, see Fig. 2(e)]. As the system reaches equilibrium, the temperature becomes uniform across the sample and the same level of demagnetization is reached on the multipicosecond time scale [C, see Fig. 2(f)]. To summarize, we identified two contributions to the wavelength dependence of the demagnetization of Co/Pt layers: first, heating at short time scales is more efficient at longer wavelength ($T_e \propto \lambda^2$) and second, subwavelength optical effects unfolding through the entire sample favor energy deposition into the magnetic domains with increasing pump wavelength, in the studied range. More studies are needed to disentangle both contributions.

Obviously, more investigation is needed to provide full insight into the light-induced, wavelength-dependent demagnetization dynamics revealed by the current experiments. Proper models should include a microscopic description of the ESP populations' dynamics and energy distribution but, as emphasized above, they should also deal properly with electromagnetic effects on the full sample scale. Microscopic effects are likely to introduce a temperature dependence for the collision frequency which, in turn, defines the conductivity and optical absorption of the materials. This would affect the wavelength dependence of the overall laser-induced demagnetization process. However, this does not affect the general conclusion of our simplified analysis, i.e., that pump wavelength scaling of laser-induced ultrafast demagnetization can only be fully assessed if regular optical principles are taken into account. Providing such a full microscopic-to-macroscopic perspective is a challenge that will be difficult to overcome in the near future.

Finally, previous reports have also identified a wavelength dependence on the demagnetization of different materials. Of those reports, Bierbrauer *et al.* [7] is the most relevant comparison to this work. They have reported time-resolved MOKE measurements on bulk nickel, for pump photon energies of 1.55 eV (0.8 μm) and 3.10 eV (0.4 μm). Our observations strongly overlap with theirs, however, with different interpretation. They have normalized the data to the maximum demagnetization and have attributed the observed wavelength dependence to different system recovery times. Renormalizing the data to the absorbed energy instead reveals that it is the maximum quenching of the magnetization that is wavelength dependent [see Fig. 2(e)].

IV. CONCLUSION

In conclusion, we have studied the effect of the pump wavelength on the ultrafast demagnetization of a Co/Pt multilayer sample. We attribute the intrinsic behavior of the magnetization at long pump-probe delays to the absorbed energy in the system, allowing a comparison completely free of uncertainties arising from the determination of the wavelength-dependent absorption and reflectivity, and of the distribution of such absorbed energy within the sample. We find that a longer wavelength quenches the magnetization on the ultrashort time scale more efficiently. Numerical analysis suggests that this observation is related to (i) a more efficient electronic heating in metals at longer laser wavelengths, and (ii) a wavelength dependence on how the energy is deposited spatially in the complex sample favoring more efficient coupling to the Co/Pt layers at $1.8 \mu\text{m}$. This work suggests routes

of optimizing the capping layer and the pump wavelength for more efficient absorption of the energy in order to drive low consumption magnetic devices.

ACKNOWLEDGMENTS

The authors warmly thank M. Hehn for providing the multilayers used in this study. The INRS team acknowledges support from NSERC, FRQNT, PRIMA, and CFI-MSI. V.C. and K.L. acknowledge NSERC. T.B. acknowledges funding from the Marie Skłodowska-Curie Grant Agreement No. 798176. C.V. acknowledges NSERC through Grant No. CCIPE 517932-17 and FRQNT for Grant No. 2019-CO-254385. The UPMC team is grateful for financial support received from the CNRS-MOMENTUM.

-
- [1] E. Beaurepaire, J.-C. Merle, A. Daunois, and J.-Y. Bigot, *Phys. Rev. Lett.* **76**, 4250 (1996).
- [2] C. Vicario, C. Ruchert, F. Ardana-Lamas, P. M. Derlet, B. Tudu, J. Luning, and C. P. Hauri, *Nat. Photonics* **7**, 720 (2013).
- [3] D. Polley, M. Pancaldi, M. Hudl, P. Vavassori, S. Urazhdin, and S. Bonetti, *J. Phys. D* **51**, 084001 (2018).
- [4] R. Gort, K. Bühlmann, S. Däster, G. Salvatella, N. Hartmann, Y. Zemp, S. Hohenstein, C. Stieger, A. Fognini, T. U. Michlmayr, T. Bähler, A. Vaterlaus, and Y. Acremann, *Phys. Rev. Lett.* **121**, 087206 (2018).
- [5] G. P. Zhang, W. Hübner, G. Lefkidis, Y. Bai, and T. F. George, *Nat. Phys.* **5**, 499 (2009).
- [6] K. Bobowski, M. Gleich, N. Pontius, C. Schüßler-Langeheine, C. Trabant, M. Wietstruk, B. Frietsch, and M. Weinelt, *J. Phys.: Condens. Matter* **29**, 234003 (2017).
- [7] U. Bierbrauer, S. T. Weber, D. Schummer, M. Barkowski, A.-K. Mahro, S. Mathias, H. Christian Schneider, B. Stadtmüller, M. Aeschlimann, and B. Rethfeld, *J. Phys.: Condens. Matter* **29**, 244002 (2017).
- [8] S. Pan, O. Hellwig, and A. Barman, *Phys. Rev. B* **98**, 214436 (2018).
- [9] S. Essert and H. C. Schneider, *Phys. Rev. B* **84**, 224405 (2011).
- [10] G. Rohde, T. Rohwer, A. Stange, C. Sohrt, K. Hanff, L. X. Yang, L. Kipp, K. Rossnagel, and M. Bauer, *J. Electron Spectros. Relat. Phenom.* **195**, 244 (2014).
- [11] B. Koopmans, G. Malinowski, F. Dalla Longa, D. Steiauf, M. Fähnle, T. Roth, M. Cinchetti, and M. Aeschlimann, *Nat. Mater.* **9**, 259 (2010).
- [12] M. Battiato, K. Carva, and P. M. Oppeneer, *Phys. Rev. Lett.* **105**, 027203 (2010).
- [13] M. Fähnle, M. Haag, C. Illg, B. Mueller, W. Weng, T. Tsatsoulis, H. Huang, J. Briones, N. Teeny, L. Zhang, and T. Kuhn, *Am. J. Mod. Phys.* **7**, 68 (2018).
- [14] K. Krieger, P. Elliott, T. Müller, N. Singh, J. K. Dewhurst, E. K. U. Gross, and S. Sharma, *J. Phys.: Condens. Matter* **29**, 224001 (2017).
- [15] P. Tengdin, W. You, C. Chen, X. Shi, D. Zusin, Y. Zhang, C. Gentry, A. Blonsky, M. Keller, P. M. Oppeneer, H. C. Kapteyn, Z. Tao, and M. M. Murnane, *Sci. Adv.* **4**, eaap9744 (2018).
- [16] A. Eschenlohr, M. Battiato, P. Maldonado, N. Pontius, T. Kachel, K. Holldack, R. Mitzner, A. Föhlisch, P. M. Oppeneer, and C. Stamm, *Nat. Mater.* **12**, 332 (2013).
- [17] W. You, P. Tengdin, C. Chen, X. Shi, D. Zusin, Y. Zhang, C. Gentry, A. Blonsky, M. Keller, P. M. Oppeneer, H. Kapteyn, Z. Tao, and M. Murnane, *Phys. Rev. Lett.* **121**, 077204 (2018).
- [18] G. Salvatella, R. Gort, K. Bühlmann, S. Däster, A. Vaterlaus, and Y. Acremann, *Struct. Dyn.* **3**, 055101 (2016).
- [19] N. Bergéard, M. Hehn, S. Mangin, G. Lengaigne, F. Montaigne, M. L. M. Laliou, B. Koopmans, and G. Malinowski, *Phys. Rev. Lett.* **117**, 147203 (2016).
- [20] B. Vodungbo, B. Tudu, J. Perron, R. Delaunay, L. Müller, M. H. Berntsen, G. Grübel, G. Malinowski, C. Weier, J. Gautier, G. Lambert, P. Zeitoun, C. Gutt, E. Jal, A. H. Reid, P. W. Granitzka, N. Jaouen, G. L. Dakovski, S. Moeller, M. P. Miniti, A. Mitra, S. Carron, B. Pfau, C. von Korff Schmising, M. Schneider, S. Eisebitt, and J. Lüning, *Sci. Rep.* **6**, 18970 (2016).
- [21] B. Vodungbo, J. Gautier, G. Lambert, A. B. Sardinha, M. Lozano, S. Sebban, M. Ducouso, W. Boutu, K. Li, B. Tudu, M. Tortarolo, R. Hawaldar, R. Delaunay, V. López-Flores, J. Arabski, C. Boeglin, H. Merdji, P. Zeitoun, and J. Lüning, *Nat. Commun.* **3**, 999 (2012).
- [22] L. Guidoni, E. Beaurepaire, and J.-Y. Bigot, *Phys. Rev. Lett.* **89**, 017401 (2002).
- [23] C. Boeglin, E. Beaurepaire, V. Halté, V. López-Flores, C. Stamm, N. Pontius, H. A. Dürr, and J.-Y. Bigot, *Nature (London)* **465**, 458 (2010).
- [24] X. Liu, Z. Xu, R. Gao, H. Hu, Z. Chen, Z. Wang, J. Du, S. Zhou, and T. Lai, *Appl. Phys. Lett.* **92**, 232501 (2008).
- [25] B. Pfau, S. Schaffert, L. Müller, C. Gutt, A. Al-Shemmary, F. Büttner, R. Delaunay, S. Düsterer, S. Flewett, R. Frömter, J. Geilhufe, E. Guehrs, C. M. Günther, R. Hawaldar, M. Hille, N. Jaouen, A. Kobs, K. Li, J. Mohanty, H. Redlin, W. F. Schlotter, D. Stickler, R. Treusch, B. Vodungbo, M. Kläui, H. P. Oepen, J. Lüning, G. Grübel, and S. Eisebitt, *Nat. Commun.* **3**, 1100 (2012).
- [26] R. H. M. M. Groeneveld, R. Sprik, and A. Lagendijk, *Phys. Rev. B* **45**, 5079 (1992).
- [27] V. Halté, J.-Y. Bigot, B. Palpant, M. Broyer, B. Prével, and A. Pérez, *Appl. Phys. Lett.* **75**, 3799 (1999).

- [28] See Supplemental Material at <http://link.aps.org/supplemental/10.1103/PhysRevB.101.054430> for a continued discussion on the alternative energy gauges and a detailed description of the experimental conditions and pump and probe pulses characterization.
- [29] A. G. Mathewson and H. P. Myers, *Phys. Scr.* **4**, 291 (1971).
- [30] W. S. M. Werner, K. Glantschnig, and C. Ambrosch-Draxl, *J. Phys. Chem. Ref. Data* **38**, 1013 (2009).
- [31] P. B. Johnson and R. W. Christy, *Phys. Rev. B* **9**, 5056 (1974).
- [32] N. Cabrera and N. F. Mott, *Rep. Prog. Phys.* **12**, 163 (1949).
- [33] N. Cai, G. Zhou, K. Müller, and D. E. Starr, *Phys. Rev. Lett.* **107**, 035502 (2011).
- [34] N. Cai, G. Zhou, K. Müller, and D. E. Starr, *Phys. Rev. B* **84**, 125445 (2011).
- [35] L. Wang, P. Han, Z. Zhang, C. Zhang, and B. Xu, *Comput. Mater. Sci.* **77**, 281 (2013).
- [36] M. Born and E. Wolf, *Principles of Optics*, 7th Ed. (Cambridge University Press, New York, 1999).

Correction: Incorrect information was used for the third affiliation, and it has been corrected.